metals

MDPI

Article

Phase Formation Features in the Metallothermal Reduction of Natural Coltan

Kirill V. Pikulin *, Stanislav N. Tyushnyakov, Roza I. Gulyaeva, Sofya A. Petrova, Andrey N. Dmitriev and Galina Yu. Vitkina *

Vatolin Institute of Metallurgy of the Ural Branch of the Russian Academy of Sciences, 101 Amundsen St., 620016 Ekaterinburg, Russia; tyushnyakov.sn@gmail.com (S.N.T.); gulroza@mail.ru (R.I.G.); danaus@mail.ru (S.A.P.); andrey.dmitriev@mail.ru (A.N.D.)

* Correspondence: pikulin.imet@gmail.com (K.V.P.); 20procents@mail.ru (G.Y.V.)

Abstract

Phase formation characteristics during the thermochemical reduction of metals from natural coltan using aluminum and calcium–aluminum alloy at 1400–1450 °C were investigated to develop methods for extracting niobium and tantalum from rare metal raw materials. The studied coltan sample consists of a columbite–tantalite solid solution with the composition $(Mn,Fe)(Nb,Ta)_2O_6$, cassiterite $Sn_{0.9}O_2$, tapiolite $(Ta,Nb)_2(Mn,Fe)O_6$, and calcioolivine Ca_2SiO_4. This study established that the choice of reducing agent determines the sequence of oxide phase transformations. During the aluminothermic process, orthorhombic columbite–tantalite is completely reduced, while tetragonal tapiolite persists even at 1400 °C. The use of a calcium–aluminum alloy containing 69.4 wt.% Ca results in a reversal of this trend: tapiolite is reduced at the early stages (800–1250 °C) through an intermediate $(Ta,Nb)O_2$ phase, whereas the columbite–tantalite solid solution remains up to 1250 °C. Calcium, having a high affinity for oxygen, forms intermediate perovskite-type oxide phases that act as diffusion barriers, limiting the access of the reducing agent to residual mineral inclusions (mainly Nb-Ta minerals of the orthorhombic crystal system). A temperature rise to 1450 °C initiates the redistribution of oxide components: the content of $CaNbO_3$ decreases, the $Ca_2(Nb,Ta)AlO_6$ phase disappears, and its components are involved in the formation of $Ca(Nb,Ta)_{0.25}MnO_{2.74}$ and $Ca_4Nb_2O_9$. Diffusion constraints are reduced, and the residual columbite–tantalite solid solution is reduced, as confirmed by its complete absence in the products at 1450 °C. In the metallic phase, solid solutions of tantalum and niobium, Ta-Nb-Sn intermetallic compounds $(Ta,Nb)_3Sn$, titanium aluminide, and ferroalloys with an increased (Ta,Nb)/(Fe,Mn) ratio are formed. The phase transformations elucidated during metallothermic reduction of coltan using different reducing agents, together with the formation of metallic and intermetallic phases, establish a scientific foundation for the development of advanced rare metal extraction processes.

Keywords: coltan; tantalum; niobium; aluminum; calcium; phase formation; metallothermic reduction

Check for updates

Academic Editor: Srecko Stopic

Received: 17 March 2026
Revised: 9 April 2026
Accepted: 15 April 2026
Published: 17 April 2026

Copyright: © 2026 by the authors. Licensee MDPI, Basel, Switzerland. This article is an open access article distributed under the terms and conditions of the Creative Commons Attribution (CC BY) license.

1. Introduction

Niobium and tantalum are classified as refractory rare metals of significant technological importance in modern industry. Due to their unique chemical and physical properties, such as corrosion and heat resistance, ductility, superconductivity, high electrical and magnetic permeability, as well as biocompatibility, these metals are widely used in various

fields of modern technology, e.g., the manufacture of heat-resistant alloys and alloyed steels, electrovacuum devices and electrolytic capacitors, medical and chemical equipment resistant to aggressive media, etc. [1–3].

Niobium and tantalum commonly occur together in various ore minerals and concentrates due to their similar physicochemical properties. More than 50 niobium and tantalum minerals are known, represented predominantly by complex oxides. From the perspective of metal extraction, the three most important groups are: the columbite–tantalite solid solution series with the general formula $(Fe,Mn)(Nb,Ta)_2O_6$; pyrochlore—$(Na,Ca,REE)_2(Nb,Ta,Ti)_2O_6(OH,F)$; and loparite—$(Na,Ca,Ce)(Ti,Nb)O_3$ [3,4]. In addition to the aforementioned minerals, ore assemblages may include tapiolite, euxenite, thoreaulite, and ilmenorutile, as well as minerals containing niobium as an isomorphic impurity (e.g., ilmenite, cassiterite, and wolframite).

In terms of niobium and tantalum content, coltan represents the most valuable raw material [5,6]. The largest coltan deposits are located in the Democratic Republic of the Congo [7,8]. The crystal structure of columbite–tantalite is described by the general formula AB_2O_6, where the A-site cation comprises an isomorphic mixture of Fe^{2+} and Mn^{2+}, while the B-site is occupied by Nb^{5+} and Ta^{5+}. The composition of the columbite–tantalite solid solution series varies widely, with Nb_2O_5 content ranging from 2 to 75 wt.% and Ta_2O_5 from 1 to 85 wt.% [4]. Minerals of this group crystallize in the orthorhombic crystal system and are chemically similar to tapiolite, which shares the same general formula but adopts a tetragonal structure [4,9].

Against the background of steadily increasing global demand for niobium and tantalum, the involvement of new deposits in industrial processing and the development of advanced technologies for manufacturing value-added products based on these metals have become critical priorities.

Numerous methods exist for extracting niobium and tantalum from ores and concentrates [10,11], as well as from industrial waste [12,13] and secondary raw materials [14,15]. Conventional coltan processing typically involves chemically aggressive conditions. The most common methods utilize hydrofluoric acid [16,17], mixed acid systems [18,19], or various alkalis [20,21]. Chlorination technology is also widely employed for processing mineral and technogenic Nb-Ta raw materials [22,23]. While these conventional methods have proven technologically and economically efficient for high-grade tantalum–niobium ores, they encounter significant difficulties when processing low-grade materials. Specifically, chlorination technology poses severe safety and environmental risks due to the use of large volumes of chlorine, rendering it economically unviable for ores with high gangue content. Similarly, hydrometallurgical processes inevitably generate significant volumes of fine-grained sludge requiring disposal or storage. Additional drawbacks include complex feed preparation, multi-stage process flows, energy-intensive evaporation operations, and wastewater neutralization requirements.

In the development of technologies for refractory rare metals, particularly tantalum and niobium, metallothermal recovery of valuable metals from low-grade complex ores and technogenic waste, followed by hydrometallurgical separation, represents a promising direction [24–29]. This concentration method relies on the selective reduction of element oxides present in the raw material, which is particularly advantageous for processing low-grade ores and concentrates. Furthermore, metallothermal reduction offers several advantages over processes such as carbothermal reduction, primarily due to its exothermic nature and simplified equipment design.

Reduction of Ta and Nb from their oxides can be achieved using reducing agents such as aluminum [24], magnesium [25,26], calcium [27,28], and silicon [29]. The metallothermal process is often conducted via self-propagating high-temperature synthesis (SHS) to obtain

powders with a high specific surface area. In contrast, the aluminothermic process yields metal in the form of ingots or pellets. Aluminum is selected as the reducing agent for rare metal oxides due to its high reactivity and relatively low cost. If the heat generated during the reaction is insufficient, or to facilitate metal–slag separation, exothermic additives (e.g., iron oxide) and fluxes (CaO, CaF_2, and SiO_2) are added to the charge.

To enhance the reduction efficiency of tantalum and niobium oxides, the use of reducing agents with high chemical activity is recommended. Calcium, possessing significant reducing power, is one of the most efficient reagents for producing tantalum and niobium. However, its application in pure form is limited by its high reactivity with air, which leads to rapid oxide film formation, complicating industrial handling. An optimal solution is the use of a calcium–aluminum master alloy, which combines the high reducing potential of calcium with the oxidation resistance of aluminum. This approach offers additional advantages: firstly, the formation of low-melting-point eutectics in the $CaO–Al_2O_3$ system, facilitating metal–slag separation; secondly, achieving a high yield of high-quality metal due to the synergistic effect of the alloy components.

The industrial implementation of the calcium–aluminothermic process was carried out at NPM Silmet OÜ (Estonia) with the objective of reducing pure niobium and tantalum oxides [28]. Nevertheless, the utilization of this technology in relation to ore-based mineral feedstock, particularly coltan, remains to be the subject of adequate scholarly scrutiny. It is imperative that research is conducted into the patterns of phase formation during the reduction of coltan, in order to develop a scientifically sound technology for the extraction of rare metals. This work is of particular relevance in this context.

This paper presents the results of a study on phase formation during the metallothermal reduction of natural coltan using aluminum and a calcium–aluminum alloy.

2. Materials and Methods

A natural coltan sample from the Democratic Republic of the Congo was used in this study; its chemical composition is presented in Table 1. The mineral was crushed to a particle size of <0.1 mm prior to experimentation. Aluminum powder of PA-4 grade (Al $\geq$ 98.0 wt.%, Fe $\leq$ 0.35 wt.%, Si $\leq$ 0.40 wt.%, and particle size < 0.14 mm) and metallic calcium (Ca $\geq$ 98.7 wt.%, Cu $\leq$ 0.01 wt.%, and particle size < 1.0 mm) were employed as reducing agents. Additionally, a calcium–aluminum master alloy was prepared by melting high-purity metals in an electric resistance furnace under an argon atmosphere at 950–1000 °C. The Ca/Al mass ratio in the alloy was maintained at 2.27:1.0. Its phase composition was characterized by the intermetallic compounds Ca_8Al_3 and $Ca_{13}Al_{14}$, and the alloy was ground to a particle size of <0.1 mm for experimental use.

Table 1. Chemical composition of the natural coltan sample.

Mineral	Content, wt.%											
	Nb	**Ta**	**Fe**	**Mn**	**Sn**	**Si**	**Al**	**Cu**	**Mg**	**Ni**	**Ti**	**Zr**
Coltan	21.18	26.74	8.29	4.86	5.90	0.81	0.62	0.36	0.78	0.34	1.19	0.11

The chemical composition of the natural coltan sample was determined by inductively coupled plasma optical emission spectrometry (ICP-OES) using a SPECTRO ARCOS spectrometer (SPECTRO Analytical Instruments GmbH, Kleve, Germany).

The phase composition and crystal structure of the natural coltan sample, as well as the products of its interaction with aluminum, calcium, or a calcium–aluminum master alloy, were determined by powder X-ray diffraction (XRD) using Rietveld refinement. Measurements were performed at room temperature on a D8 ADVANCE diffractometer

(«Bruker AXS GmbH», Karlsruhe, Germany) equipped with a VÅNTEC-1 position-sensitive detector («Bruker AXS GmbH», Karlsruhe, Germany), using Cu Kα radiation (34 kV, 40 mA) and a β-filter. Diffraction patterns were collected over a 2θ range of 5–100° with a step size of 0.021° and a counting time of 3284 s per step. Phase identification and structural analysis were carried out using the ICDD PDF-4+ database.

The microstructure and elemental composition of the natural coltan sample were characterized by scanning electron microscopy (SEM) and energy-dispersive X-ray spectroscopy (EDS) using a TESCAN MIRA 3 LMU microscope (TESCAN ORSAY HOLDING, Brno, Czech Republic) equipped with an Oxford Instruments INCA Energy 350 system (Oxford Instruments plc, Abingdon, Oxfordshire, UK) and an X-max 80 silicon drift detector (TESCAN ORSAY HOLDING, Brno, Czech Republic). The phase identification for minerals was established based on the correlation of three independent datasets: (1) local elemental composition obtained by EDS; (2) morphology and contrast observed in BSE mode; and (3) crystallographic parameters determined by Rietveld refinement for the bulk sample.

Phase transformations during the metallothermal reduction process were investigated using simultaneous thermal analysis (STA) with NETZSCH STA 449 C Jupiter (NETZSCH-Gerätebau GmbH, Selb, Germany) and STA 449 F3 Jupiter instruments (NETZSCH-Gerätebau GmbH, Selb, Germany). Measurements were performed during heating to 800–1460 °C and subsequent cooling at a rate of 20 °C/min under a flow of high-purity argon (99.998%). The compositions of the samples used for thermal analysis are presented in Table 2.

Table 2. Composition of coltan-reductant mixtures used for thermal analysis: heating at 20 °C/min to target temperatures (t_{max}) under flowing argon.

Experiment No	Charge Composition, wt.%				t_{max}, °C
	Coltan	Al	Ca-Al Master Alloy	Ca	
1	79.7	20.3	–	–	1400
2	77.8	17.8	–	4.4	1400
3	69.4	–	30.6	–	800
4					1250
5					1460

3. Results and Discussion

According to XRD data (Figure 1), the studied coltan sample consists of the following minerals: 80.0 wt.% columbite–tantalite solid solution with the composition $(Mn,Fe)(Nb,Ta)_2O_6$, 8.0 wt.% cassiterite $Sn_{0.9}O_2$, 7.5 wt.% tapiolite $(Ta,Nb)_2(Mn,Fe)O_6$, and 4.5 wt.% calcioolivine Ca_2SiO_4. The columbite–tantalite solid solution and calcioolivine crystallize in the orthorhombic crystal system with space groups Pbcn (ICDD PDF-4 04-005-8824) and Pmmn (ICDD PDF-4 04-012-6734), respectively, whereas cassiterite and tapiolite belong to the tetragonal crystal system (space group $P4_2/mnm$). The unit cell parameters for all identified minerals are listed in Table 3. Based on the general formula AB_2O_6 for columbite–tantalite and the dependence of unit cell parameters on the Fe/Mn ratio [30], the proportions of iron and manganese were estimated to be 0.46 and 0.54, respectively.

SEM-EDS analysis revealed the chemical compositions of various mineral phases within the coltan sample corresponding to the columbite–tantalite group (Figure 2, Table 4). The sample matrix predominantly consists of medium-grained columbite $(Mn_{0.56}Fe_{0.44})(Nb_{0.69}Ta_{0.31})_2O_6$ with a niobium content up to 41.9 wt.%, and tantalite $(Mn_{0.38}Fe_{0.62})(Nb_{0.47}Ta_{0.53})_2O_6$ enriched in tantalum (up to 51.8 wt.% Ta). Niobium-free tapiolite particles with the composition $(Mn_{0.17}Fe_{0.83})Ta_2O_6$, containing iron (up to 9.5 wt.%) and manganese (up to 2.1 wt.%), were also identified. Additionally, medium-sized wodgi-

nite inclusions $(Mn_{0.48}Fe_{0.52})(Sn_{0.67}Nb_{0.33})Ta_2O_8$ containing approximately 13.0 wt.% Sn were detected. In addition to structurally bound tin, discrete cassiterite (SnO_2) particles were observed. Associated gangue minerals in the sample include hematite, ilmenite (Ti ≈ 29.0 wt.%), kyanite, quartz, and zircon (41.7 wt.% Zr, 9.6 wt.% Hf).

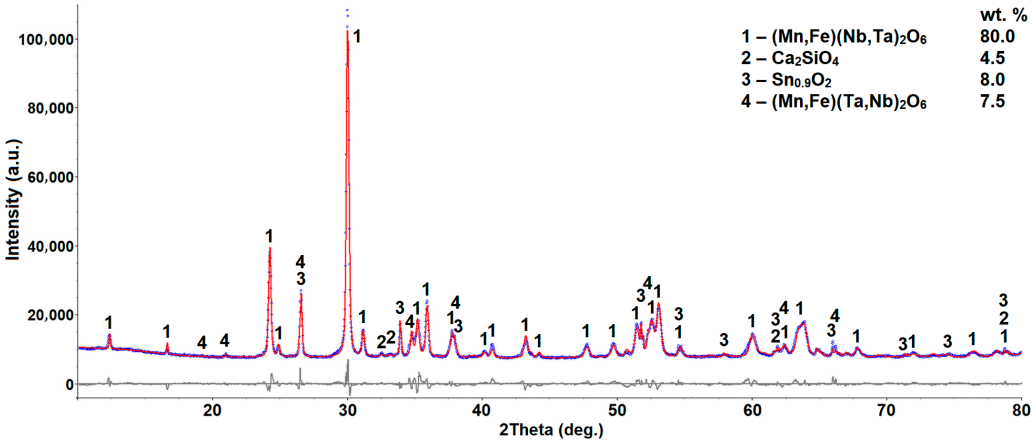


Figure 1. Observed and calculated XRD patterns, difference curve for the natural coltan sample (Refinement parameters: Rwp = 3.85%, Rp = 2.64%, and GOF = 3.85).

Table 3. Phase composition and unit cell parameters of phases in the natural coltan sample.

No	Mineral/ Formula	Unit Cell Parameters				Content, wt.%	PDF4 Cards
		a (Å)	b (Å)	c (Å)	V (Å^3)		
1	Columbite–tantalite/ $(Mn,Fe)(Nb,Ta)_2O_6$	14.3003 (8)	5.7410 (3)	5.0982 (3)	418.55 (4)	80.0	04-005-8824
2	Calcioolivine/ Ca_2SiO_4	6.734 (8)	5.515 (7)	9.30 (1)	345.2 (7)	4.5	04-012-6734
3	Cassiterite/ $Sn_{0.9}O_2$	4.7387 (2)	–	3.1839 (2)	71.50 (1)	8.0	01-070-4176
4	Tapiolite/ $(Mn,Fe)(Ta,Nb)_2O_6$	4.7551 (4)	–	9.214 (1)	208.33 (4)	7.5	04-011-1021

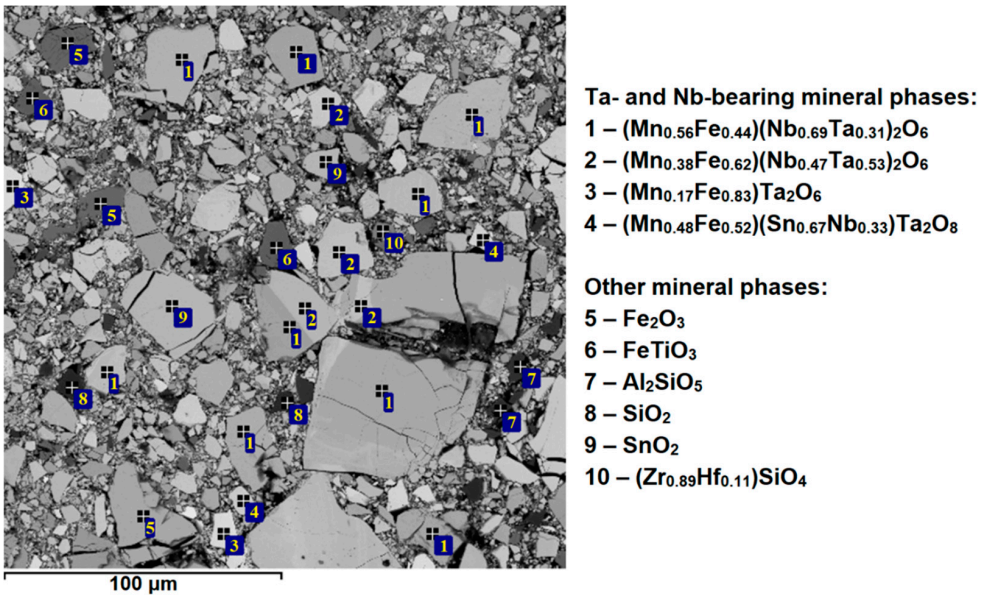


Figure 2. Microstructure of natural coltan particles with EDS analysis points.

Table 4. Local elemental composition of identified mineral phases determined by EDS.

Points	Element Content, wt.% (Min-Max)/Mean Value									Mineral/Chemical Formula
	O	Al	Si	Ti	Mn	Fe	Nb	Sn	Ta	
1	22.9–26.8 24.9	– –	– –	– –	3.9–11.7 7.8	1.0–9.3 5.2	22.6–41.9 32.3	– –	17.6–42.4 30.0	Columbite/ $(Mn_{0.56}Fe_{0.44})(Nb_{0.69}Ta_{0.31})_2O_6$
2	21.7–23.5 22.6	– –	– –	– –	3.7–8.1 5.9	3.8–8.7 6.3	13.8–26.5 20.2	0.0–1.4 0.7	37.6–51.8 44.7	Tantalite/ $(Mn_{0.38}Fe_{0.62})(Nb_{0.47}Ta_{0.53})_2O_6$
3	19.1–19.2 19.2	– –	– –	– –	1.4–2.1 1.8	8.3–9.5 8.9	– –	– –	69.9–70.4 70.2	Tapiolite/ $(Mn_{0.17}Fe_{0.83})Ta_2O_6$
4	21.6–23.1 22.4	– –	– –	0.0–0.6 0.3	2.9–5.3 4.1	3.3–6.1 4.7	2.6–7.1 4.9	12.4–13.1 12.8	47.8–54.1 51.0	Wodginite/ $(Mn_{0.48}Fe_{0.52})(Sn_{0.67}Nb_{0.33})Ta_2O_8$
5	31.0–33.4 32.2	– –	– –	0.0–7.0 3.5	– –	59.6–69.0 64.3	– –	– –	– –	Hematite/ Fe_2O_3
6	35.4–36.2 35.8	– –	– –	28.3–29.5 28.9	1.4–2.7 2.1	32.8–33.7 33.3	– –	– –	– –	Ilmenite/ $FeTiO_3$
7	48.1–48.9 48.5	29.1–29.6 29.4	13.9–14.0 14.0	– –	– –	7.7–8.0 7.9	– –	– –	– –	Cyanite/ Al_2SiO_5
8	52.7–52.9 52.8	– –	47.1–47.3 47.2	– –	– –	– –	– –	– –	– –	Quartz/ SiO_2
9	21.1–21.2 21.2	– –	– –	– –	– –	– –	– –	77.6–78.8 78.2	0.0–1.2 0.60	Cassiterite/ SnO_2
10 *	33.6	0.2	14.3	–	–	0.6	–	–	–	Zircon/ $(Zr_{0.89}Hf_{0.11})SiO_4$

* means 41.7% Zr, 9.6% Hf.

According to thermal analysis data, the DSC thermogram of the studied coltan sample exhibited two endothermic effects (Figure 3): the first, a weak effect with onset/peak temperatures of 1361/1409 °C, was attributed to the orthorhombic-to-tetragonal phase transition of columbite–tantalite [31], while the second, with a peak at 1467 °C, corresponded to mineral melting. Upon cooling, exothermic effects associated with crystallization and the reverse phase transition were observed at onset/peak temperatures of 1442/1437 °C and 1364/1355 °C, respectively.

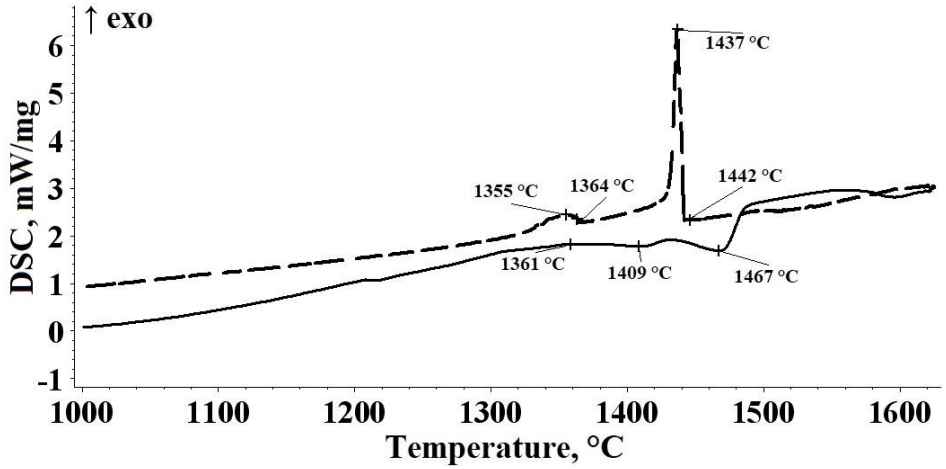


Figure 3. DSC thermogram showing heat flow of natural coltan: heating cycle (solid line) and cooling cycle (dashed line) at 20 °C/min under flowing argon.

Experimental investigation of the interaction between natural coltan and aluminum, with the aluminum content calculated for complete metal reduction (25.5 wt.% Al), demonstrated that heating of the reaction mixture on the DSC thermogram (Figure 4) is accompanied by an endothermic effect attributed to aluminum melting (onset/peak temperatures:

650/660 °C). Subsequent heating to 1400 °C resulted in an exothermic effect with onset/peak temperatures of 984/1168 °C, associated with the reduction of metal oxides. No pronounced thermal effects were detected during the cooling of the reaction products.

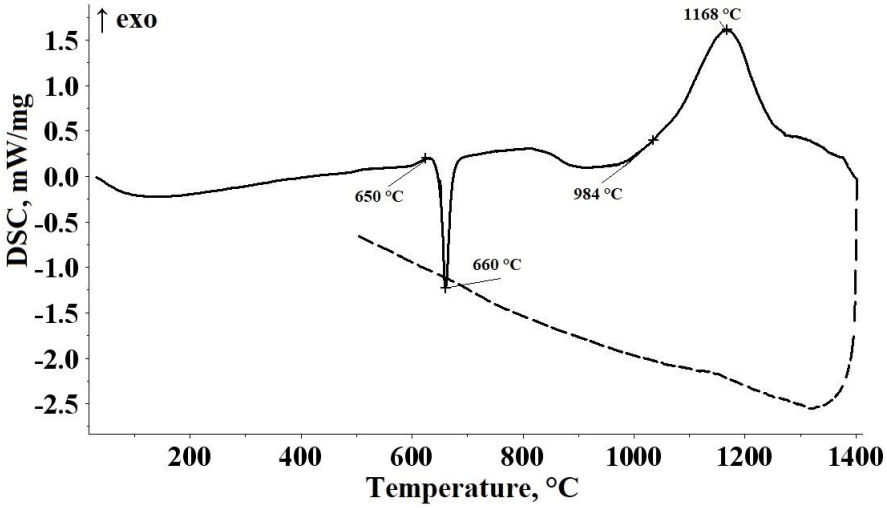


Figure 4. DSC thermogram of aluminothermic reduction of natural coltan (25.5 wt.% Al) during heating (solid line) and cooling (dashed line) at 20 °C/min under flowing argon.

According to X-ray diffraction (XRD) data (Figure 5, Table 5), the products of aluminothermic reduction of coltan after heating to 1400 °C comprise a multicomponent mixture including intermetallic compounds (Ta,Nb)FeAl and (Ta,Nb)Sn, a (Ta,Nb) solid solution, the (Nb,Ta)(Fe,Mn)$_2$ and (Zr,Nb)$_2$Al phases, as well as oxide compounds: corundum (Al_2O_3), tetragonal tapiolite ((Fe,Mn)(Nb,Ta)$_2O_6$), and metastable niobium monoxide (NbO).

The presence of NbO in the products indicates the stepwise nature of the reduction of niobium-containing phases, attributed to localized aluminum deficiency due to its consumption in aluminide formation.

As demonstrated in the Materials Project database and the relevant literature [32], the Nb-O system comprises multiple stable phases: Nb_2O_5, NbO_2, and NbO. The reduction of niobium pentoxide by aluminum is a process that occurs in stages.

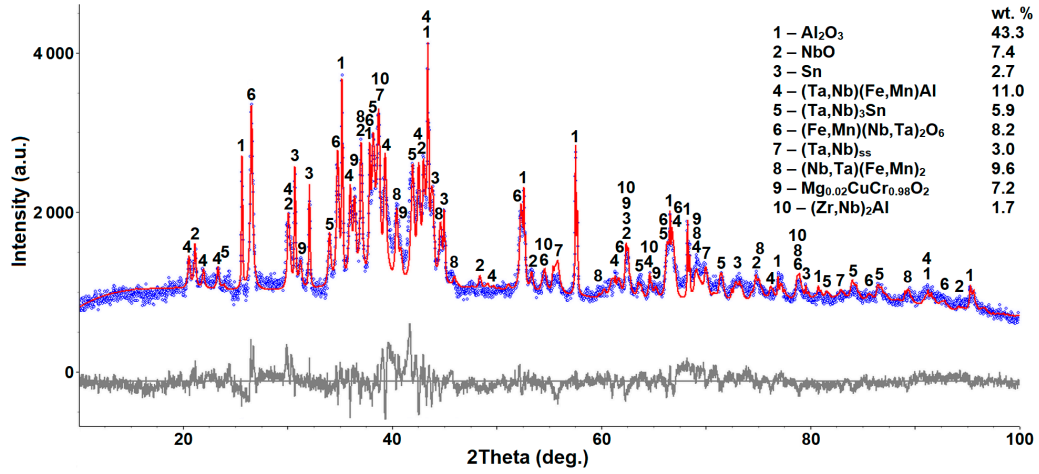


Figure 5. Observed and calculated XRD patterns, difference curve for the aluminothermic reduction products of natural coltan (25.5 wt.% Al) at 1400 °C (Refinement parameters: Rwp = 8.60%, Rp = 6.42%, and GOF = 2.93).

Table 5. Phase composition and unit cell parameters of phases in the aluminothermic reduction products of natural coltan (25.5 wt.% Al) at 1400 °C.

No	Phase	Spatial Group	Unit Cell Parameters			Content, wt.%	Cards PDF4
			a (Å)	c (Å)	V (Å^3)		
1	Al_2O_3	R-3c	4.758	12.993	254.77	43.3	04-010-6477
2	NbO	Pm-3m	4.210	–	74.60	7.4	04-008-3657
3	Sn	I41/amd	5.831	3.181	108.16	2.7	04-004-7747
4	(Ta,Nb)(Fe,Mn)Al	P63/mmc	4.997	8.112	175.42	11.0	04-001-5964
5	$(Ta,Nb)_3Sn$	Pm-3n	5.278	–	147.05	5.9	04-023-4737
6	$(Fe,Mn)(Nb,Ta)_2O_6$	$P4_2/mnm$	4.757	9.220	208.67	8.2	01-074-2182
7	$(Ta,Nb)_{ss}$	Im-3m	3.293	–	35.70	3.0	04-001-2738
8	$(Nb,Ta)(Fe,Mn)_2$	P63/mmc	4.857	7.906	161.53	9.6	04-003-3920
9	$Mg_{0.02}CuCr_{0.98}O_2$	R-3m	2.979	17.198	132.15	7.2	04-015-2954
10	$(Zr,Nb)_2Al$	P63/mmc	4.681	5.783	109.74	1.7	04-003-9852

Experimental evidence has been provided to confirm the following sequence of reactions: $Nb_2O_5 \rightarrow NbO_2 \rightarrow NbO \rightarrow Nb$. During the aluminothermic reduction of Nb_2O_5, the sequential formation of NbO_2 (at ~550 °C) and NbO (at ~700 °C) was observed prior to the formation of the metal [32].

A key feature of the process is the differential behavior of the initial coltan mineral phases: orthorhombic columbite–tantalite (space group Pbcn) was completely reduced, forming metals, ferroalloys, and intermetallic compounds, whereas tetragonal tapiolite (space group $P4_2/mnm$) was retained at 8.2 wt.% with unit cell parameters close to the initial values (a = 4.757 Å, c = 9.220 Å). This indicates the increased resistance of tantalum-rich mineral domains to aluminothermic reduction. This behavior is attributed to the crystallochemical features of the phases: tapiolite, unlike columbite, is characterized by a high tantalum content (up to 85 wt.% Ta_2O_5 [4]) and, similar to pyrochlore [33], exhibits stronger Ta–O bonds compared to Nb–O bonds. Consequently, the reducibility of columbite–tantalite group minerals by aluminum increases with increasing niobium content, as manifested in the sequence: tapiolite → columbite. The observed trend is consistent with kinetic data on the carbothermic reduction of Ta,Nb-containing minerals, where tantalum-rich phases exhibit a lower degree of metal recovery compared to niobium-rich phases at 1200–1400 °C [34].

In the present study, the phase formation during the aluminothermic reduction of coltan at temperatures below 1400 °C was not the subject of investigation.

Therefore, it is not possible to determine the sequence of formation of intermediate oxides in the initial phase of the reaction directly. Nonetheless, in consideration of the DSC data (exothermic peaks in the 900–1168 °C range), the presence of suboxides (NbO) in the products at 1400 °C, and data from the literature [35], the following macro-mechanism of interaction can be proposed. The process is initiated at 660 °C, which is the temperature at which aluminum melts. This is accompanied by the formation of physical contact between the liquid reducing agent and the surface of the coltan mineral grains, as well as the wetting of the oxide surface by the aluminum melt.

Subsequently, active reduction and phase formation (660–1168 °C) occur. Within the temperature range corresponding to exothermic effects on the DSC curve (maximum at 1168 °C), a vigorous interaction is observed. The process is exothermic and rapid, and as a consequence, the principal reactions proceed in parallel, rather than strictly sequentially. The reduction process commences with phases that are enriched in niobium (columbite–tantalite solid solution), given that the Nb–O bonds are weaker than the Ta–O bonds.

The schematic equation for the initial reduction can be represented as follows:

$$(Mn,Fe)(Nb,Ta)_2O_6 + Al \rightarrow NbO + (Nb,Ta) + (Mn,Fe) + Al_2O_3. \quad (1)$$

Concurrent reactions are also observed. As the metals are subjected to reduction, they react with each other and with aluminum according to the following mechanisms:

$$(Mn,Fe) + (Nb,Ta) \rightarrow (Nb,Ta)(Fe,Mn)_2, \quad (2)$$

$$(Mn,Fe) + (Nb,Ta) \rightarrow (Ta,Nb)(Fe,Mn)Al. \quad (3)$$

Simultaneously, the associated tin (cassiterite) undergoes a reduction process in stages and binds refractory metals, as evidenced by data from [36]:

$$3SnO_2 + 2Al = 3SnO + Al_2O_3, \quad (4)$$

$$3SnO + 2Al = 3Sn + Al_2O_3, \quad (5)$$

$$(Ta,Nb) + Sn \rightarrow (Ta,Nb)3Sn. \quad (6)$$

The process is then said to reach completion, accompanied by a further reduction of oxides and the homogenization of the metal melt.

The presence of residual tapioite in the products, as the phase richest in tantalum, is consistent with the data from a study demonstrating the interaction of reducing agents with natural tantalite [35].

The partial replacement of aluminum with calcium (19.8 wt.% Ca) significantly alters the nature of the interaction between coltan and the reducing agent, as reflected in the DSC thermogram (Figure 6). The interaction of the components is initiated after aluminum melting and appears as an intense combined exothermic peak with an onset at 668 °C and a maximum at 704 °C. This effect is probably attributed to the formation of calcium–aluminum intermetallic compounds (e.g., Al_4Ca and Al_2Ca), which form at the boundary of the liquid Al-Ca phase [37]. Subsequently, the resulting mixture of intermetallic compounds and residual aluminum melt acts as an active reducing agent, providing the reduction of the oxide components of natural coltan. The reduction processes proceed through several stages, observed as exothermic peaks at 815 °C, 989 °C, 1200 °C, and 1310 °C, indicating the sequential course of complex multiphase reactions from partial reduction to the formation of final metallic and oxide phases.

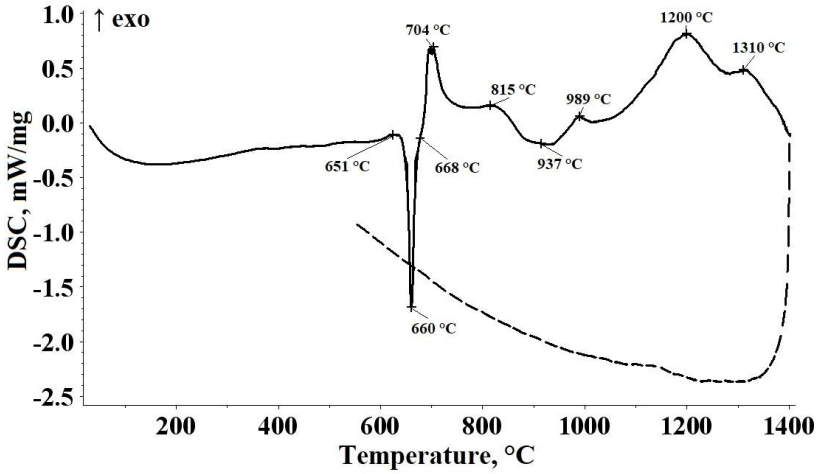


Figure 6. DSC thermogram of aluminothermic reduction of natural coltan (25.5 wt.% Al) during heating (solid line) and cooling (dashed line) at 20 °C/min under flowing argon.

According to XRD results (Figure 7, Table 6), the oxide component of the products from the interaction of natural coltan with an aluminum–calcium mixture after heating to 1400 °C under argon atmosphere was found to contain a mayenite phase ($Ca_{12}Al_{14}O_{33}$, space group I-43d) in addition to corundum (Al_2O_3). A key feature, in contrast to aluminothermic reduction, is the absence of tapiolite and the formation of a tetragonal oxide $(Ta,Nb)O_2$ (space group $P4_2/mnm$), while residual amounts of orthorhombic columbite–tantalite solid solution remain. The results obtained indicate a predominant interaction of calcium, as well as Ca-Al intermetallic compounds, with tetragonal Ta-Nb minerals. The formation of a tantalum–niobium oxide solid solution probably occurs during the reduction stage of tetragonal tapiolite. In contrast to aluminothermic reduction, the calcium–aluminothermic reducibility of columbite–tantalite group minerals increases with increasing tantalum content, as follows: columbite → tapiolite.

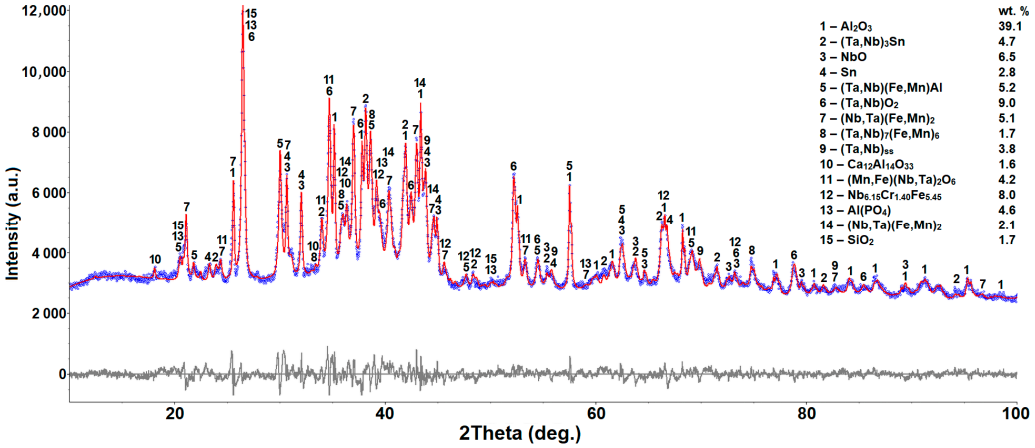


Figure 7. Observed and calculated XRD patterns, difference curve for the reduction products of natural coltan with an aluminum–calcium mixture (19.8 wt.% Ca) at 1400 °C (Refinement parameters: Rwp = 3.84%, Rp = 2.95%, and GOF = 2.29).

Table 6. Phase composition and unit cell parameters of phases in the reduction products of natural coltan with an aluminum–calcium mixture (19.8 wt.% Ca) at 1400 °C.

No	Phase	Spatial Group	Unit Cell Parameters			Content wt.%	Cards PDF4
			a (Å)	c (Å)	V(Å^3)		
1	Al_2O_3	R-3c	4.756	12.990	254.47	39.1	04-015-8995
2	$(Ta,Nb)_3Sn$	Pm-3n	5.272	–	146.54	4.7	04-004-5091
3	NbO	Pm-3m	4.208	–	74.51	6.5	04-005-6079
4	Sn	I41/amd	5.829	3.180	108.08	2.8	04-003-2197
5	(Ta,Nb)(Fe,Mn)Al	P63/mmc	4.984	8.146	175.20	5.2	04-001-5964
6	$(Ta,Nb)O_2$	P42/mnm	4.759	3.078	69.71	9.0	04-002-3935
7	$(Nb,Ta)(Fe,Mn)_2$	P63/mmc	4.859	7.905	161.65	5.1	04-001-7266
8	$(Ta,Nb)_7(Fe,Mn)_6$	R-3m	5.015	27.809	605.66	1.7	04-001-3106
9	$(Ta,Nb)_{ss}$	Im-3m	3.295	–	35.77	3.8	04-003-5516
10	$Ca_{12}Al_{14}O_{32.5}$	I-43d	11.992	–	1724.65	1.6	04-015-0819
11 *	$(Mn,Fe)(Nb,Ta)_2O_6$	Pbcn	14.194	5.133	417.72	4.2	04-012-3522
12	$Nb_{6.15}Cr_{1.40}Fe_{5.45}$	R-3m	4.940	26.958	569.64	8.0	04-022-6431
13	$Al(PO_4)$	P3121	5.005	10.609	230.13	4.6	04-009-5761
14	$(Nb,Ta)(Fe,Mn)_2$	P63/mmc	4.848	7.855	159.87	2.1	04-017-9960
15	SiO_2	P3121	4.922	5.363	112.53	1.7	04-005-4718

* b = 5.734 Å.

The metallic phase contained (Table 6) iron- and manganese-bearing tantalum–niobium aluminides ((Ta,Nb)(Fe,Mn)Al), tantalum–niobium solid solutions, a tantalum–

niobium–tin intermetallic compound with the structure $(Ta,Nb)_3Sn$ (space group Pm-3m), as well as ferroalloys with varying (Ta,Nb)/(Fe,Mn) ratios, specifically $(Ta,Nb)(Fe,Mn)_2$ and $(Ta,Nb)_7(Fe,Mn)_6$. The presence of the $(Ta,Nb)_7(Fe,Mn)_6$ phase when using a mixture of reducing agents, and its absence in the conventional aluminothermic process, indicates more efficient reduction of tantalum and niobium when employing an aluminum–calcium mixture.

When a calcium—aluminum master alloy (69.4 wt.% Ca) was used as a reducing agent in combination with natural coltan, the DSC thermogram (Figure 8) exhibited an endothermic effect with onset/peak temperatures of 535/543 °C, attributed to melting of the eutectic component in the alloy. A combined exothermic effect with a pronounced maximum at 657 °C was attributed to phase transformations within the alloy and the reduction of tapiolite, resulting in the formation of tantalum–niobium oxide solid solutions. X-ray diffraction analysis of intermediates obtained by heating the reagent mixture to 800 °C (Figure 9, Table 7) revealed that, as a result of the interactions, the alloy composition shifted toward $CaAl_2$, indicating aluminum enrichment. Additionally, CaO formed during reduction reacted with SnO_2 to produce calcium stannate ($CaSnO_3$).

Further heating to 1250 °C results in intensive reduction of metals from the oxide components of natural coltan, as evidenced by exothermic effects with maxima at 923 and 1108 °C. In the temperature range of 800–1250 °C (Figure 9, Table 7), solid solutions of tantalum and niobium, a tantalum–niobium–tin intermetallic compound $(Ta,Nb)_3Sn$, titanium aluminide Ti_3Al, as well as ferroalloys with varying (Ta,Nb)/(Fe,Mn) ratios are formed in the metallic phase. The formation of intermetallic compounds with an A15 (Nb_3Sn) structure is consistent with the data presented in [38], which investigated phase equilibria in the Al–Nb–Sn system at 900 and 1200 °C. The findings demonstrated the stability of the A15 phase within the specified temperature range and the high solubility of tin in Nb_2Al. As demonstrated in [39,40], the existence of the Laves phase Fe_2Nb and the μ-phase Fe_7Nb_6 at temperatures ranging from 1200 to 1450 °C is evidenced by the available data on ferroalloys and iron intermetallides. Despite a significant decrease in the content of orthorhombic columbite–tantalite solid solution in the reaction products, its residual amount remains, whereas tetragonal tapiolite is completely absent in the final products. In addition, a significant difference between calcium–aluminothermic reduction and the conventional aluminothermic process is the formation of intermediate oxide phases with a perovskite-type structure $Ca_2(Nb,Ta)AlO_6$ and $CaNbO_3$. These compounds serve as diffusion barriers that restrict the access of the reducing agent to the residual mineral inclusions of columbite–tantalite, thereby slowing down the final stage of reduction.

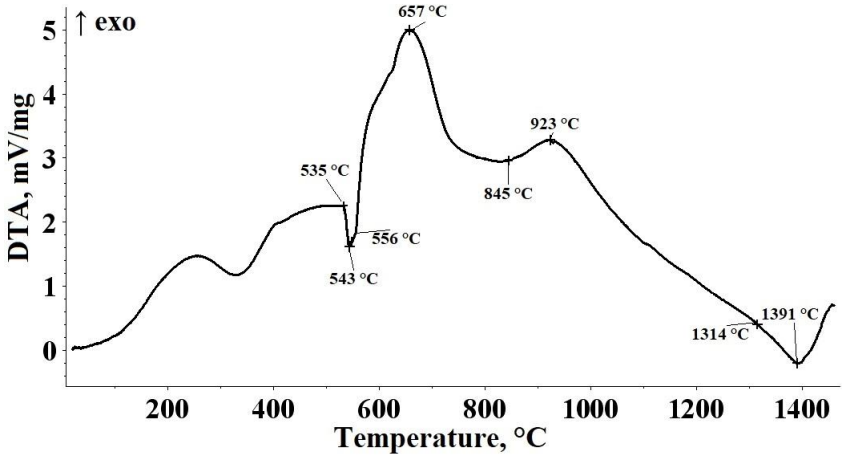


Figure 8. DSC thermogram of coltan reduction by a calcium–aluminum master alloy during heating at 20 °C/min under flowing argon.

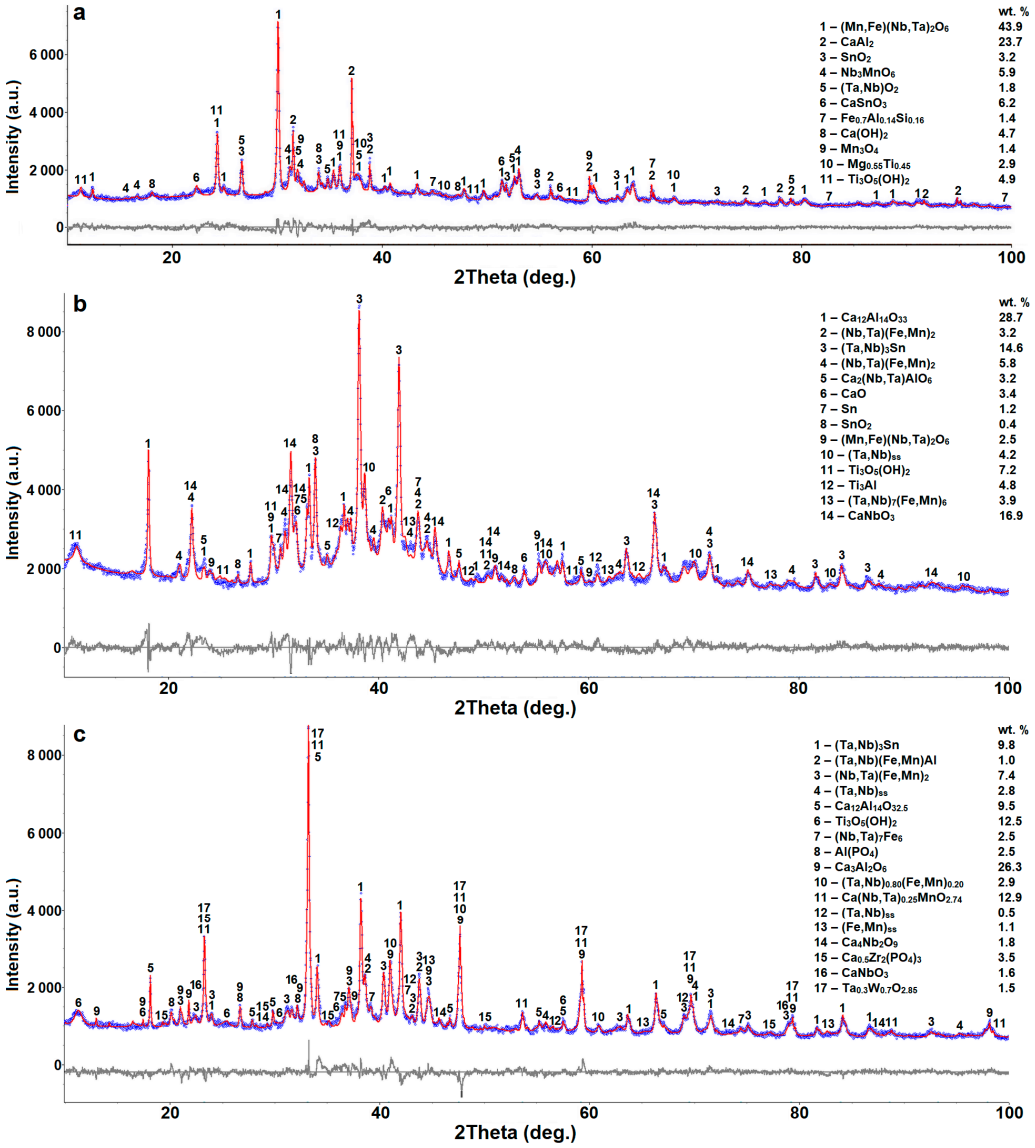


Figure 9. Observed and calculated XRD patterns, difference curves for reduction products of natural coltan with a calcium–aluminum master alloy at 800 °C (**a**), 1250 °C (**b**), and 1450 °C (**c**) (Refinement parameters: (**a**) Rwp = 5.37%, Rp = 4.24%, and GOF = 1.78, (**b**) Rwp = 4.86%, Rp = 3.78%, and GOF = 2.18, and (**c**) Rwp = 5.88%, Rp = 4.48%, and GOF = 1.94).

According to XRD data, the products of coltan heating with a calcium–aluminum master alloy to 1450 °C (Figure 9, Table 7) showed the complete disappearance of Ti_3Al, which was previously present in the reduction products at 1250 °C. However, there was an increase in the content of reduced titanium oxide in the form of $Ti_3O_5(OH)_2$, formed during storage as a result of air exposure. This phenomenon indicates that titanium aluminide can act as a reducing agent when heated to 1450 °C. The resulting alumina (Al_2O_3) is involved in the formation of calcium aluminates during reduction.

The most significant changes occur in the niobium-containing oxide subsystem. The $CaNbO_3$ content sharply decreases from 16.9 to 1.6 wt.%, accompanied by the complete disappearance of the residual columbite–tantalite solid solution. Instead, a Nb-poor, Mn- and Ca-rich phase with the composition $Ca(Nb,Ta)_{0.25}MnO_{2.74}$, and a calcium niobate with high CaO content, $Ca_4Nb_2O_9$, are formed. Within the oxide matrix, calcium oxide is redistributed to form more thermodynamically stable high-temperature compounds. The released CaO and newly formed alumina (Al_2O_3) initiate recrystallization of the aluminate

bonding phase. A transformation of the mayenite phase ($Ca_{12}Al_{14}O_{32.5}$) was observed: its content decreased from 28.7 to 9.5 wt.%, while tricalcium aluminate ($Ca_3Al_2O_6$) formed in an amount of 26.3 wt.%.

Table 7. Phase composition of reduction products from natural coltan using a Ca–Al master alloy at different heating temperatures (800–1450 °C) under argon.

No	Phase	Spatial Group	The Content in the Products (wt.%) After Heating to a Temperature (°C)			Cards PDF4
			800	1250	1450	
1	$(Mn,Fe)(Nb,Ta)_2O_6$	Pbcn	43.9	2.5	-	04-014-2992 04-012-3522
2	$CaAl_2$	Fd-3m	23.7	-	-	04-012-6338
3	SnO_2	P42/mnm	3.2	0.4	-	04-003-0974
4	Nb_3MnO_6	Immm	5.9	-	-	04-012-6976
5	$(Ta,Nb)O_2$	P42/mnm	1.8	-	-	04-004-3018
6	$CaSnO_3$	Pnma	6.3	-	-	04-007-8720
7	$Fe_{0.7}Al_{0.14}Si_{0.16}$	Im-3m	1.4	-	-	04-018-7279
8	$Ca(OH)_2(CaO)$	P-3m1	4.7	3.4	-	04-010-3117 (04-006-5940)
9	Mn_3O_4	I41/amd	1.4	-	-	04-015-2577
10	$Mg_{0.55}Ti_{0.45}$	Im-3m	2.9	-	-	04-017-5241
11	$Ti_3O_5(OH)_2$	C2/m	4.9	7.2	12.5	04-021-8783
12	$Ca_{12}Al_{14}O_{32.5}$	I-43d	-	28.7	9.5	04-015-0819
13	$(Nb,Ta)(Fe,Mn)_2$	P63/mmc	-	9.0	7.4	04-017-9960 04-001-7266
14	$(Ta,Nb)_3Sn$	Pm-3n	-	14.6	9.8	04-004-5091
15	$Ca_2(Nb,Ta)AlO_6$	P21/n	-	3.2	-	04-014-0990
16	Sn	I41/amd	-	1.2	-	04-004-7747
17	$(Ta,Nb)_{ss}$	Im-3m	-	4.2	2.8	04-003-5516
18	Ti_3Al	P63/mmc	-	4.8	-	04-003-0974
19	$(Ta,Nb)_7(Fe,Mn)_6$	R-3m	-	3.9	2.5	04-012-3522
20	$CaNbO_3$	Pnma	-	16.9	1.6	04-001-9017
21	(Ta,Nb)(Fe,Mn)Al	P63/mmc	-	-	1.0	04-001-5964
22	$Al(PO_4)$	P3121	-	-	2.5	04-004-6777
23	$Ca_3Al_2O_6$	Pa-3	-	-	26.3	04-001-3106
24	$(Ta,Nb)_{0.80}(Fe,Mn)_{0.20}$	Fm-3m	-	-	2.9	04-007-3583
25	$Ca(Nb,Ta)_{0.25}MnO_{2.74}$	Pm-3m	-	-	12.9	04-020-8945
26	$(Fe,Mn)_{ss}$	Im-3m	-	-	1.1	04-016-6734
27	$Ca_4Nb_2O_9$	P21/c	-	-	1.8	04-017-5651
28	$Ca_{0.5}Zr_2(PO_4)_3$	R-3c	-	-	3.5	04-005-5489
29	$Ta_{0.3}W_{0.7}O_{2.85}$	Pm-3m	-	-	1.5	04-008-4357

In the context of a Ca-Al alloy, the process exhibits a slightly divergent macromechanism. In the initial reduction stage (up to 800 °C), the interaction between coltan and the Ca-Al alloy occurs via the formation of intermediate oxide phases. In the process of reduction, a portion of the niobium present in tapioite reacts with oxygen to form dioxide. This reaction subsequently combines with manganese, resulting in the formation of Nb_3MnO_6. The overall initial reaction is thus represented as follows (where the Ca-Al alloy is denoted as $Ca_{0.604}Al_{0.396}$):

$$(Mn,Fe)(Nb,Ta)_2O_6 + Ca_{0.604}Al_{0.396} \rightarrow (Ta,Nb)O_2 + Nb_3MnO_4 + (Fe,Al) + CaO + Al_2O_3. \quad (7)$$

Concurrently, cassiterite reacts with calcium oxide (CaO) according to the following reaction:

$$SnO_2 + CaO = CaSnO_3. \quad (8)$$

Concurrently, the alloy components are converted into $CaAl_2$, which subsequently acts as the primary reducing agent.

The following reaction equations (or diagrams) can be used to represent the process of heating the reaction mixture to 1250 °C:

$$(Mn,Fe)(Nb,Ta)_2O_6 + CaAl_2 \rightarrow (Mn,Fe) + (Nb,Ta) + CaO + Al_2O_3 \quad (9)$$

$$(Mn,Fe)(Nb,Ta)_2O_6 + CaAl_2 \rightarrow (Mn,Fe) + (Nb,Ta) + Ca_2(Nb,Ta)AlO_6 + Al_2O_3 \quad (10)$$

$$3CaSnO_3 + 2CaAl_2 = 3Sn + 5CaO + 2Al_2O_3 \quad (11)$$

$$3(Nb, Ta) + Sn = (Nb, Ta)_3Sn, \quad (12)$$

$$(Nb, Ta) + (Fe, Mn) \rightarrow (Nb, Ta)_x(Fe, Mn)_y, \quad (13)$$

where x and y represent the fractions of (Nb, Ta) and (Fe, Mn) in the ferroalloy composition, respectively.

Subsequent reduction is achieved through the involvement of the established intermetallic compounds of coltan impurity elements (Ti_3Al), aluminum dissolved in the solid solution (Nb, Ta), and calcium vapor. In [41], calcium sublimation above 1000 °C was observed during the study of the interaction between $FeNb_2O_6$ and Ca. A similar phenomenon appears to be characteristic of the interaction between coltan and the ligature. As indicated by XRF data, a substantial redistribution of components transpires at temperatures in excess of 1450 °C. A complete disappearance of titanium aluminide is observed, which can be schematically represented by the following equations:

The following reactions are possible:

$$(Mn,Fe)(Nb,Ta)_2O_6 + Ti_3Al \rightarrow (Nb,Ta)_x(Fe,Mn)_y + Ti_3O_5 + Al_2O_3, \quad (14)$$

$$(Mn,Fe)(Nb,Ta)_2O_6 + Al \rightarrow (Nb,Ta)_x(Fe,Mn)_y + (Ta,Nb)(Fe,Mn)Al + Al_2O_3. \quad (15)$$

The following reaction may occur with calcium pairs:

$$2Ca_2(Ta,Nb)AlO_6 + 5Ca = 2(Ta,Nb) + 9CaO + Al_2O_3. \quad (16)$$

$$3CaNbO_3 + Ca = Ca_4Nb_2O_9 + Nb. \quad (17)$$

Concurrently, a redistribution of components occurs within the CaO-Al_2O_3 system.

A generalized interaction diagram of natural coltan with various reducing agents heated to 1400 and 1450 °C, shown in Figure 10, illustrates the key differences in phase formation between aluminothermic and calcium–aluminothermic reduction processes. Elucidating these mechanisms enables the identification of critical factors determining the efficiency of niobium and tantalum extraction. The conventional aluminothermic process dictates the reduction sequence based on the strength of the metal–oxygen chemical bond. Since the Ta–O bond is thermodynamically more stable than the Nb–O bond, tetragonal tapiolite (enriched in tantalum) retains its structure even at 1400 °C, whereas orthorhombic columbite–tantalite is completely reduced. In contrast, when using a Ca–Al master alloy, an inversion of this process is observed. Calcium, with its high affinity for oxygen and ability to form stable niobates, alters the thermodynamic potential of the system. Tapiolite is reduced in the early stages (800–1250 °C) via an intermediate $(Ta,Nb)O_2$ oxide phase and is completely absent from the product mixture at 1250 °C. The role of perovskite-like phases as diffusion barriers in the Ca–Al alloy system is a pivotal factor in the observed inversion of the reduction sequence. It appears that, at the "coltan–perovskite" interface, the limiting step is the diffusion of the reducing agent through the layer of forming perovskite

towards the reaction front. The observed delay in the reduction of columbite–tantalite at 1250 °C and its intensification at 1450 °C, when the perovskite phases undergo structural transformations, is consistent with the hypothesis. Simultaneously formed calcium niobate acts as a diffusion barrier, restricting the access of the reducing agent to residual inclusions of orthorhombic columbite–tantalite. Raising the temperature to 1450 °C initiates the redistribution of oxide components, accompanied by the completion of the reduction of residual columbite–tantalite.

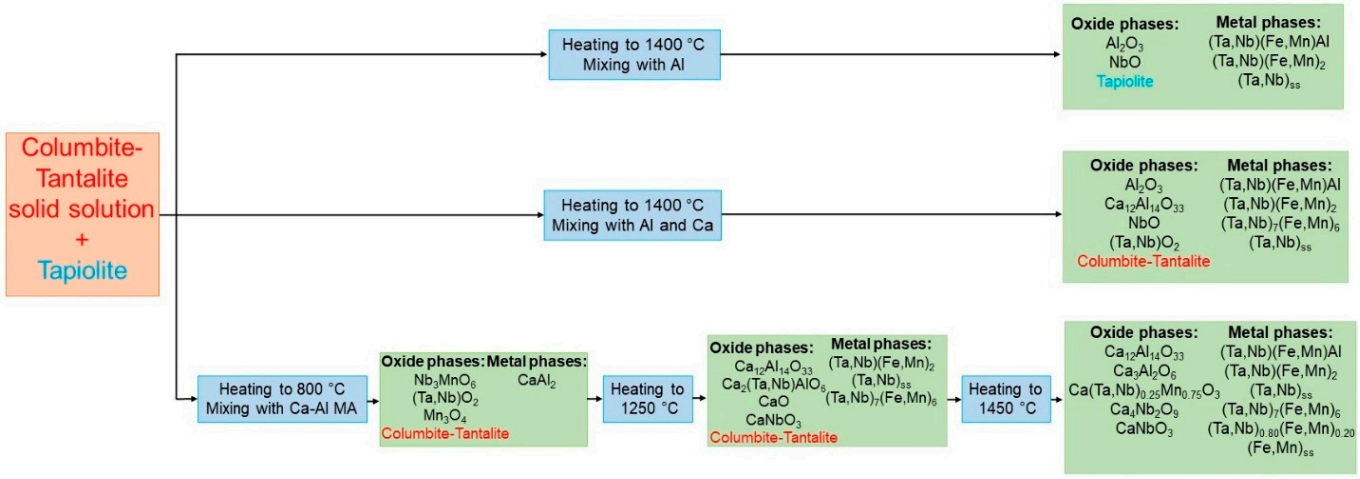


Figure 10. Generalized interaction diagram of natural coltan with various reducing agents heated to 1400–1450 °C.

The results obtained contribute to the development of theoretical understanding of the mechanisms of phase formation during metallothermal reduction of tantalum- and niobium-containing natural raw materials. The use of aluminum as a reducing agent is associated with several limitations. The high thermodynamic stability of the system promotes the formation of aluminides in the metallic phase, resulting in significant aluminum content in the final product and significantly complicating subsequent refining stages required to obtain the target metals.

The use of a calcium–aluminum master alloy as a reducing agent overcomes these limitations. Calcium, with its high chemical activity, ensures more complete extraction of tantalum and niobium into the metallic phase. Furthermore, the calcium oxide formed during the reduction process interacts with refractory corundum (α-Al_2O_3), forming low-temperature eutectics in the CaO–Al_2O_3 system.

4. Conclusions

1. The mechanism of phase formation during the metallothermal reduction of niobium and tantalum from natural coltan using aluminum, a calcium–aluminum mixture, and a Ca–Al master alloy as reducing agents has been elucidated.
2. It has been established that the reduction of coltan by aluminum during heating is limited by the crystallochemical stability of the initial minerals. Selective phase transformations are observed with stoichiometric consumption of the reducing agent: the orthorhombic columbite–tantalite solid solution is completely reduced, whereas tetragonal tapiolite remains preserved in the reduction products up to 1400 °C. The interaction products are a multicomponent mixture consisting of (Ta,Nb) metallic solid solutions, ferroalloys with a low (Ta,Nb)/(Fe,Mn) ratio, and aluminides of the (Ta,Nb)(Fe,Mn)Al system. The oxide component of the products consists mainly of corundum (Al_2O_3), niobium suboxide (NbO), and residual tapiolite.

3. The use of a Ca–Al master alloy fundamentally changes the process kinetics, causing an inversion of the reduction sequence of columbite–tantalite group minerals. Unlike aluminothermy, tapiolite is reduced in the early stages (up to 1250 °C) via intermediate oxide solid solutions, whereas the complete decomposition of columbite–tantalite requires heating to 1450 °C. A distinctive feature of the process is the formation of intermediate perovskite-type niobate phases, which are absent during conventional aluminum reduction. At 1250 °C, the system is dominated by mayenite ($Ca_{12}Al_{14}O_{32.5}$) and calcium niobate ($CaNbO_3$). Increasing the temperature to 1450 °C leads to the final reduction of the residual columbite–tantalite solid solution with the release of manganese-containing phases, resulting in the formation of a perovskite-like phase $Ca(Nb,Ta)_{0.25}MnO_{2.74}$, accompanied by a parallel decrease in the $CaNbO_3$ content. The released components are redistributed: calcium oxide is consumed for the synthesis of high-temperature tricalcium aluminate ($Ca_3Al_2O_6$) instead of mayenite, as well as for the formation of calcium-enriched niobate $Ca_4Nb_2O_9$.
4. The results obtained may be utilized for the development of metallothermal extraction processes for niobium and tantalum from natural columbite; however, quantitative assessment of process efficiency requires additional metallurgical testing with physical separation of the metallic and slag phases.
5. The following areas have been identified as offering significant potential for research: The first stage of the research involved the detailed kinetic modeling of the process, including the calculation of activation energies and the identification of rate-limiting steps. The second stage involved the investigation of phase evolution using in situ high-temperature X-ray diffraction methods to monitor transformations in real time. The third stage involved conducting pilot-scale laboratory tests to optimize the charge composition (type of reducing agent and fluxing additives) and process operating parameters, in order to identify the optimal process operating parameters.

Author Contributions: Conceptualization, K.V.P. and S.N.T.; methodology, R.I.G. and S.A.P.; software, S.A.P. and G.Y.V.; provided equipment and key reagents for research, R.I.G. and S.A.P.; validation, K.V.P. and A.N.D.; investigation, S.N.T. and G.Y.V.; data curation, K.V.P. and S.N.T.; writing—original draft preparation, K.V.P. and R.I.G.; writing—review and editing, A.N.D. and G.Y.V.; prepared figures and visualizations, G.Y.V. and S.A.P.; project administration, K.V.P.; funding acquisition, K.V.P. and A.N.D. All authors have read and agreed to the published version of the manuscript.

Funding: This work was supported by the Russian Science Foundation (grant No 25-79-00206).

Data Availability Statement: The original contributions presented in this study are included in the article. Further inquiries can be directed to the corresponding authors.

Acknowledgments: This research was carried out using the equipment of the Center for Collective Use "Ural-M". The authors would like to express their sincere gratitude to Svetlana V. Sergeeva for her valuable consultations in the field of thermal analysis.

Conflicts of Interest: The authors declare no conflicts of interest.

References

1. Rajak, D.K.; Jordaan, R.; Gomez-Arias, A.; Purcell, W. Extractive metallurgy of columbite-tantalite ore: A detailed review. *Miner. Eng.* **2022**, *190*, 107917. [CrossRef]
2. Mackay, D.A.R.; Simandl, G.J. Geology, market and supply chain of niobium and tantalum—A review. *Miner. Depos.* **2014**, *49*, 1025–1047. [CrossRef]
3. Shikika, A.; Sethurajan, M.; Muvundja, F.; Mugumaoderha, M.C.; Gaydardzhiev, S. A review on extractive metallurgy of tantalum and niobium. *Hydrometallurgy* **2020**, *198*, 105496. [CrossRef]
4. Nzeh, N.S.; Adeosun, S.; Popoola, A.P.; Adeleke, A.; Okanigbe, D. Process applications and challenges in mineral beneficiation and recovery of niobium from ore deposits—A review. *Miner. Process. Extr. Metall. Rev.* **2022**, *43*, 833–864. [CrossRef]

5. Shikika, A.; Zabene, F.; Muvundja, F.; Mugumaoderha, M.C.; Colaux, J.L.; Aatach, M.; Gaydardzhiev, S. Extraction of Ta and Nb from a coltan bearing ore by means of ammonium bifluoride fluorination and sulphuric acid leaching. *Minerals* **2021**, *11*, 1392. [CrossRef]
6. Magdalena, R.; Calvo, G.; Valero, A. The energy cost of extracting critical raw materials from tailings: The case of coltan. *Geosciences* **2022**, *12*, 214. [CrossRef]
7. Hayes, K.; Burge, R. *Coltan Mining in the Democratic Republic of Congo: How Tantalum-Using Industries Can Commit to the Reconstruction of the DRC*; Fauna & Flora International: Cambridge, UK, 2003; pp. 1–60.
8. Mantz, J.W. Improvisational economies: Coltan production in the Eastern Congo. *Soc. Anthropol.* **2008**, *16*, 34–50. [CrossRef]
9. Ercit, T.S. Hidden story of tapiolite. *Mineral. Mag.* **2010**, *74*, 715–729. [CrossRef]
10. Nzeh, N.S.; Mokgalaka, M.; Maila, N.; Popoola, P.; Okanigbe, P.; Adeleke, A.; Adeosun, S. Pyrometallurgical approach in the recovery of niobium and tantalum. In *Extraction Metallurgy-New Perspectives*; IntechOpen: London, UK, 2022. [CrossRef]
11. Haile, M.G.; Oyelola, A.O.; Aramide, F.O.; Seidu, S.O.; Akinlabi, O. Hydrometallurgical, pyrometallurgical and electrometallurgical extraction of niobium and tantalum: An overview. *Miner. Process. Extr. Metall.* **2025**, *134*, 1. [CrossRef]
12. Rodriguez, O.; Alguacil, F.J.; Baquero, E.E.; Garcia-Diaz, I.; Fernandez, P.; Sotillo, B.; Lopez, F.A. Recovery of niobium and tantalum by solvent extraction from Sn-Ta-Nb mining tailings. *RSC Adv.* **2020**, *10*, 21406–21412. [CrossRef]
13. Allain, E.; Kanari, N.; Diot, F.; Yvon, J. Development of a process for the concentration of the strategic tantalum and niobium oxides from tin slags. *Miner. Eng.* **2019**, *134*, 97–103. [CrossRef]
14. Kurylak, W. *Innovation Potential in the Recovery of Refractory Metals from Urban Mines*; D4.3 Contract #688993 Report; Multi-Stakeholder Platform for a Secure Supply of Refractory Metals in Europe; 2016; pp. 1–51. Available online: https://prometia.eu/wp-content/uploads/2020/12/MSP-REFRAM-D4.3-Innovation-potential-in-the-recovery-of-refractory-metals-from-urban-mines.pdf (accessed on 17 March 2026).
15. Kolobov, G.A.; Panov, V.S.; Rakova, N.N. Technologies of secondary refractory rare metals (review). *Russ. J. Non-Ferrous Met.* **2014**, *55*, 141–147. [CrossRef]
16. Htwe, H.H.; Lwin, K.T. Study on extraction of niobium oxide from columbite-tantalite concentrate. *World Acad. Sci. Eng. Technol.* **2008**, *46*, 133–135. [CrossRef]
17. Rodriguez, M.; Quiroga, O.; Ruiz, M.C. Kinetic study of ferrocolumbite dissolution in hydrofluoric acid medium. *Hydrometallurgy* **2007**, *85*, 87–94. [CrossRef]
18. Agulyanski, A. *The Chemistry of Tantalum and Niobium Fluoride Compounds*; Elsevier Science: Lehavim, Israel, 2004; pp. 1–408.
19. Maiorov, V.G.; Nikolaev, A.I.; Kopkov, V.K.; Elizarova, I.R. Tantalite treatment process at the Congo deposit and columbite at the Zashikhinsk deposit. *Theor. Found. Chem. Eng.* **2016**, *50*, 547–553. [CrossRef]
20. Hazek, M.N.; Mohamed, N.H.; Gabr, A.A. Potash breakdown of poly-mineralized niobium-tantalum-lanthanides ore material. *Am. J. Anal. Chem.* **2019**, *10*, 103–111. [CrossRef]
21. Maiorov, A.G.; Nikolaev, A.I.; Kopkov, V.K.; Elizarova, I.P. On alkaline opening of columbite and tantalite. *Russ. J. Appl. Chem.* **2011**, *84*, 1694–1697. [CrossRef]
22. Brocchi, E.A.; Moura, F.J. Chlorination methods applied to recover refractory metals from tin slags. *Miner. Eng.* **2008**, *21*, 150–156. [CrossRef]
23. Petukhov, M.A.; Rakova, N.N.; Chub, A.V. Investigation of the process of chlorination of tantalite-columbite concentrates. *Russ. J. Non-Ferrous Met.* **2007**, *48*, 194–202. [CrossRef]
24. Munter, R.; Parshin, A.; Yamshchikov, L.; Plotnikov, V.; Gorkunov, V.; Kober, V. Reduction of tantalum pentoxide with aluminium and calcium: Thermodynamic modeling and scale skilled tests. *Proc. Est. Acad. Sci.* **2010**, *59*, 243–252. [CrossRef]
25. Hong, J.; Hwang, S.; Kang, N.; Lee, D. Comparison of the magnesiothermic reduction behavior of Nb_2O_5 and $Ti_2Nb_{10}O_{29}$. *Metals* **2023**, *13*, 1743. [CrossRef]
26. Hwang, S.M.; Wang, J.P.; Lee, D.W. Extraction of tantalum powder via the magnesium reduction of tantalum pentoxide. *Metals* **2019**, *9*, 205. [CrossRef]
27. Baba, M.; Ono, Y.; Suzuki, R.O. Tantalum and niobium powder preparation from their oxides by calciothermic reduction in the molten $CaCl_2$. *J. Phys. Chem. Solids* **2004**, *66*, 466–470. [CrossRef]
28. Gorkunov, V.; Munter, R. Calcium-aluminothermal production of niobium and mineral composition of the slag. *Proc. Est. Acad. Sci.* **2007**, *56*, 142–156. [CrossRef]
29. Sidorenko, G.A.; Solntseva, L.S.; Gorzhevskaya, S.A. Crystallochemical study of minerals of the columbite-tantalite series. *Proc. Fersman Mineral. Mus.* **1971**, *20*, 140–154. (In Russian)
30. Awasthi, A.; Bhatt, Y.J.; Krishnamurthy, N.; Ueda, Y.; Garg, S.P. The reduction of niobium and tantalum pentoxides by silicon in vacuum. *J. Alloys Compd.* **2001**, *315*, 187–192. [CrossRef]
31. Mansurova, A.N.; Gulyaeva, R.I.; Chumarev, V.M.; Petrova, S.A. High-temperature heat capacity and temperatures of phase transformations of the $FeNb_2O_6$. *J. Alloys Compd.* **2017**, *2008*, 2409–2419. [CrossRef]

32. Mostaan, H.; Karimzadeh, F.; Abbasi, M.H. Non-isothermal kinetic studies on the formation of Al_2O_3/Nb composite. *Thermochim. Acta* **2010**, *511*, 32–36. [CrossRef]
33. Radhakrishnan, A.N.; Prabhakar Rao, P.P.; Mahesh, S.K.; Vaisakhan Thampi, D.S.; Koshy, P. Role of bond strength on the lattice thermal expansion and oxide ion conductivity in quaternary pyrochlore solid solutions. *Inorg. Chem.* **2012**, *51*, 2409–2419. [CrossRef]
34. Chumarev, V.M.; Mar'evich, V.P.; Mansurova, A.N.; Kozhakhmetov, S.M. Phase formation and the kinetics of metals reduction during the interaction of columbite, tantalite, and wodginite with carbon. *Russ. Metall.* **2008**, *2*, 10–15. [CrossRef]
35. Gulyaeva, R.I.; Udoeva, L.Y.; Petrova, S.A.; Sergeeva, S.V.; Pikulin, K.V.; Agafonov, S.N. Phase transformation during metallothermic reduction of tantalite. *Metallurgist* **2022**, *66*, 75–85. [CrossRef]
36. Tyushnyakov, S.N.; Gulyaeva, R.I.; Udoeva, L.Y.; Sergeeva, S.V.; Petrova, S.A. Metallothermic reduction of natural cassiterite. *Metallurgist* **2021**, *65*, 746–759. [CrossRef]
37. Ozturk, K.; Zhong, Y.; Chen, L.-Q.; Liu, Z.-K.; Sofo, J.O.; Wolverton, C. Linking first-principles energetics to CALPHAD: An application to thermodynamic modeling of the Al–Ca binary system. *Metall. Mater. Trans. A* **2005**, *A36*, 5–13. [CrossRef]
38. Papadimitriou, I.; Chatzitheodorou, E.; Giannakopoulos, K.; Lekatou, A.; Zervaki, A.; Tsakiropoulos, P. Phase Equilibria in the Nb-Rich Region of Al-Nb-Sn at 900 and 1200 °C. *Materials* **2019**, *12*, 2759. [CrossRef] [PubMed]
39. Voß, S.; Palm, M.; Stein, F.; Raabe, D. Phase equilibria in the Fe-Nb system. *J. Phase Equilibria Diffus.* **2011**, *32*, 97–104. [CrossRef]
40. Chu, Q.; Zhang, L.; Xia, T.; Cheng, P.; Zheng, J.; Zhang, M.; Li, J.; Yan, F.; Yan, C. Microstructure and fracture toughness of Fe–Nb dissimilar welded joints. *Metals* **2021**, *11*, 86. [CrossRef]
41. Sergeeva, S.V.; Gulyaeva, R.I.; Udoeva, L.Y.; Petrova, S.A.; Tyushnyakov, S.N. Thermodynamic simulation and experimental investigation of the calciothermic reduction of metals from manganese and iron niobates. *Russ. Metall. (Met.)* **2022**, *2022*, 909–918. [CrossRef]

Disclaimer/Publisher's Note: The statements, opinions and data contained in all publications are solely those of the individual author(s) and contributor(s) and not of MDPI and/or the editor(s). MDPI and/or the editor(s) disclaim responsibility for any injury to people or property resulting from any ideas, methods, instructions or products referred to in the content.